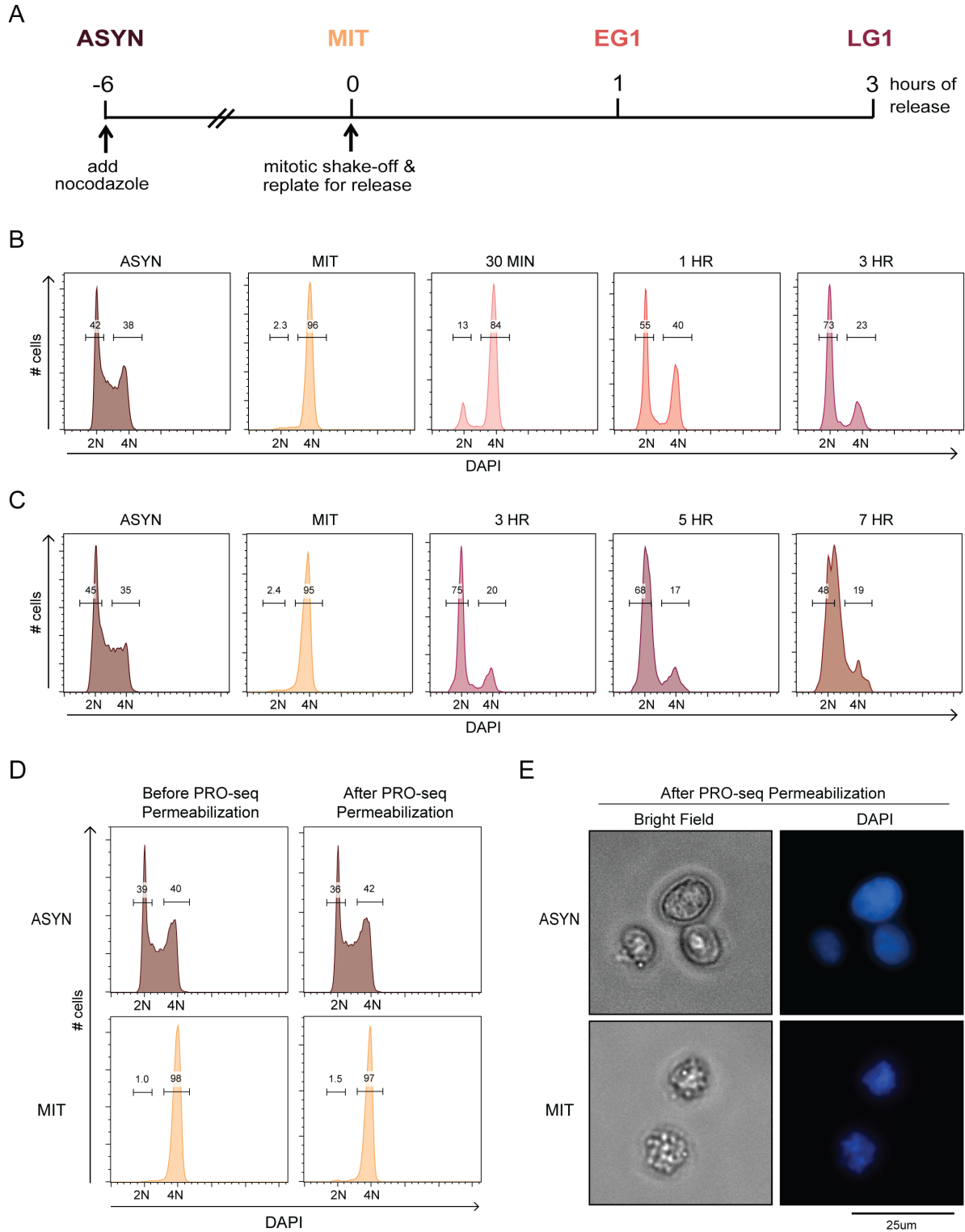


# SUPPLEMENTAL INFORMATION

Figure S1



**Figure S1. Characterization of mitotic release timing and cell purity after PRO-seq permeabilization (related to Figures 1 [panels A-C] and 2 [panels D-E])**

(A) Experimental design for mitotic release time course.

(B and C) Representative FACS histograms showing the percent of cells with a DNA content of 2N (G1) and 4N (G2/M) cells in mitotic release time courses with either an earlier time point (B) or later time points (C), which were used to select 1hr and 3hr as the best time points for EG1 and LG1, respectively.

(D) FACS plots showing percent of cells with DNA content of 2N (G1) or 4N (G2/M) for MIT and ASYN samples both before and after PRO-seq permeabilization.

(E) Representative bright field and DAPI images of MIT and ASYN cells after PRO-seq permeabilization.

Figure S2

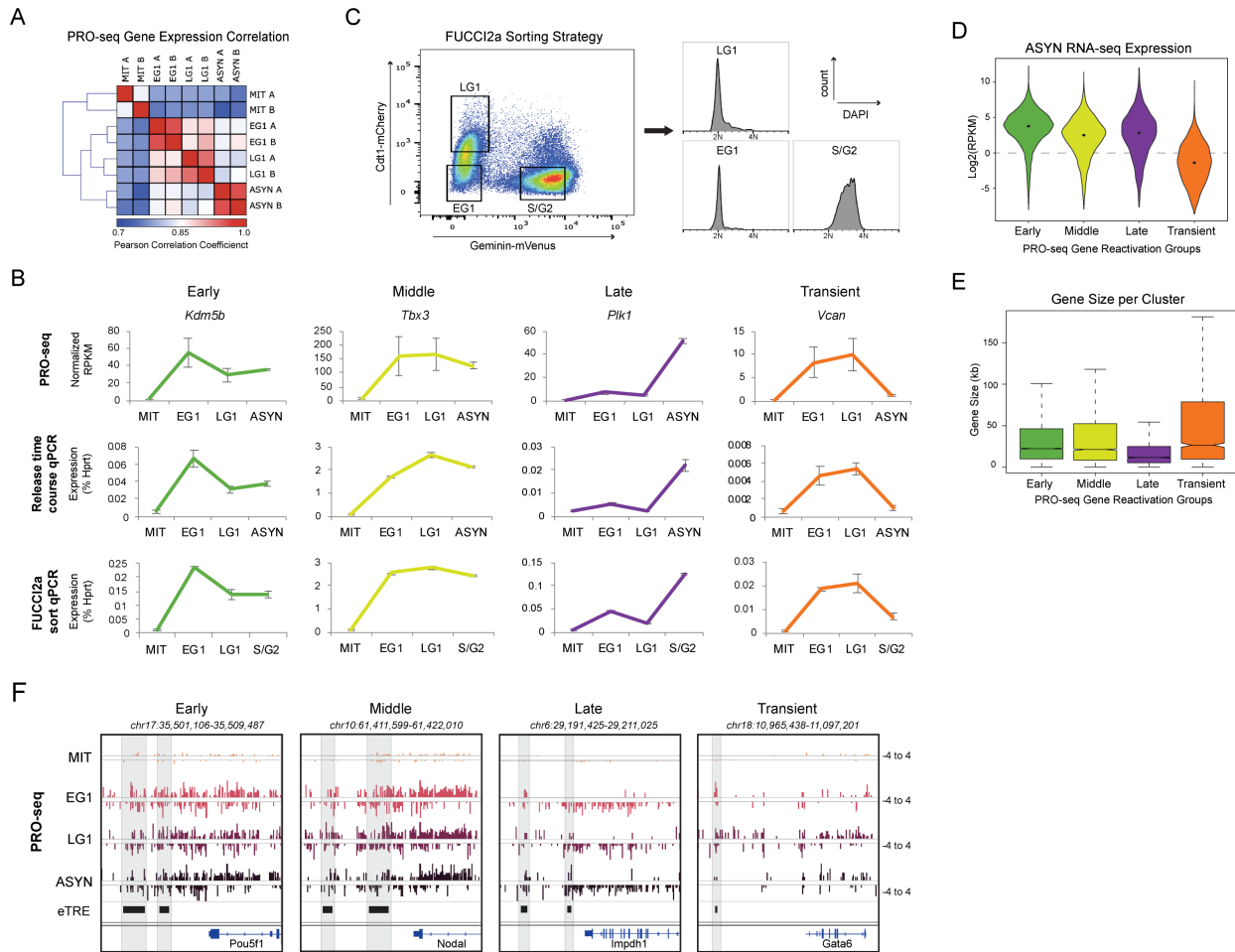


**Figure S2. Validation of PRO-seq gene reactivation clusters (related to Figure 2)**

(A) Heatmap showing the Pearson correlation among all PRO-seq samples for the 14861 protein coding genes expressed LG1 (normalized RPKM >1) in at least one time point.

(B) Validation of kinetics for one example gene in each reactivation group. Top: PRO-seq expression at each time point, average of two biological replicates. Middle: pre-mRNA qPCR from two independent mitotic release time courses. Bottom: pre-mRNA qPCR from two independent experiments using the Fucci2a sorting strategy in (C). MIT samples in all cases were obtained by synchronization and mitotic shake-off. Error bars show +/- SEM.

(C) Sorting strategy utilizing the Fucci2a system (Mort et al., 2014) to obtain pure populations of cells in EG1 (Cdt1<sup>-</sup>, Gmn<sup>-</sup>), LG1 (Cdt1<sup>+</sup>, Gmn<sup>-</sup>), and S/G2 (Gmn<sup>+</sup>). Prior to sorting, cells underwent a partial synchronization and release (without mitotic shake-off)

to enrich for cells in G1 (see methods). Histograms show the distribution of cells with a DNA content of 2N (G1) and 4N (G2/M) for each sorted population.

(D) Violin plots depicting the median and density of asynchronous RNA-seq expression ( $\text{Log}_2(\text{RPKM})$ ) for each gene reactivation group.

(E) Box plots showing the median gene size (kb) for each reactivation group.

(F) Genome browser tracks showing PRO-seq data (one replicate, plus and minus strands) for one or more eTREs from each reactivation group. Each eTRE is highlighted in gray, and the closest gene by linear distance is also shown.

Figure S3

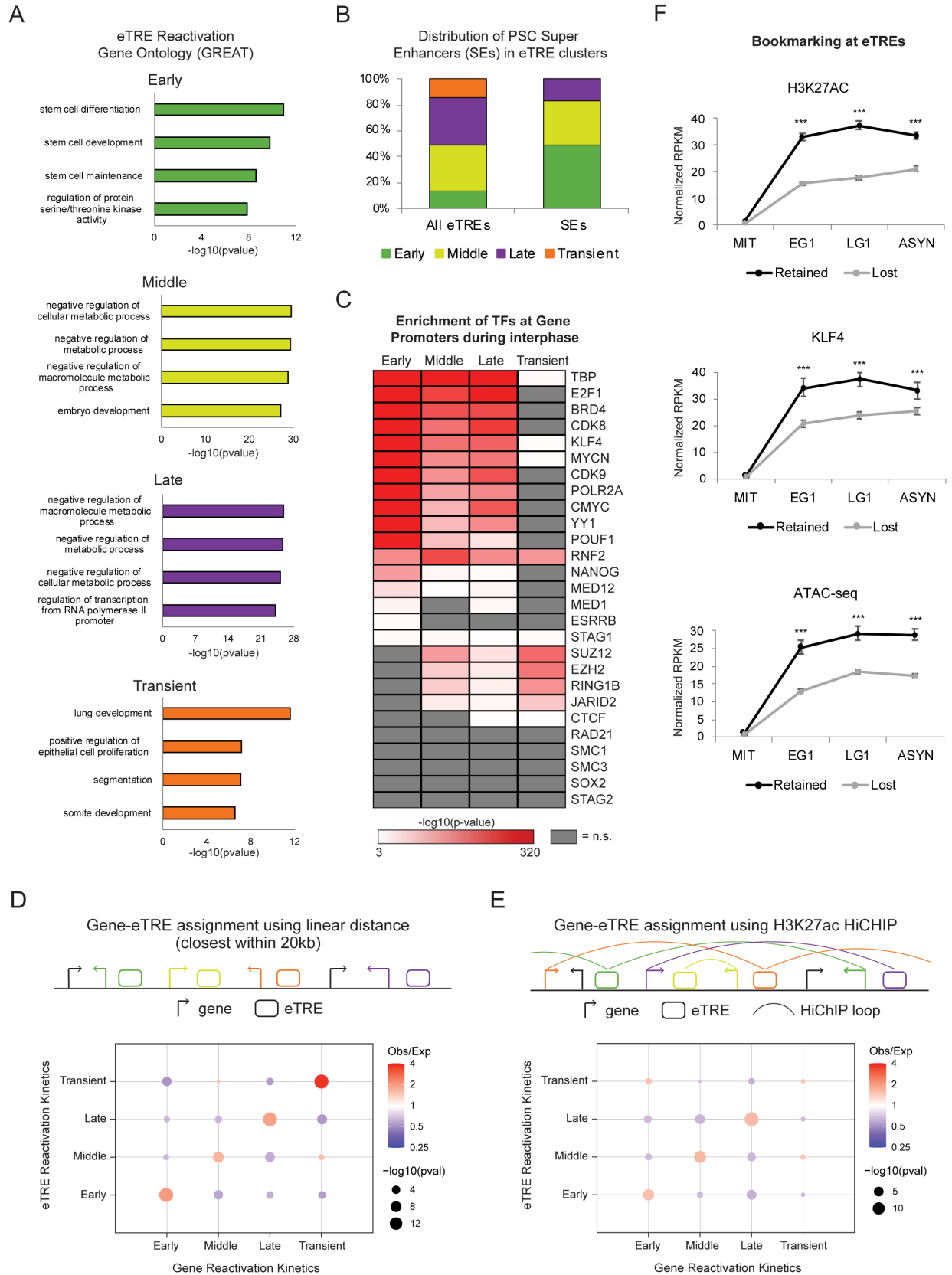


**Figure S3. Characterization of gene and eTRE reactivation clusters, coordinated resetting of gene-eTRE pairs, and correlation with mitotic bookmarking (related to Figure 3)**

(A) Bar plots show the enrichment ( $-\log_{10}(\text{pvalue})$ ) of the top four Gene Ontology (GO) terms for each eTRE transcriptional reactivation cluster, based on GREAT analysis (McLean et al., 2010). Corrected pvalue (Hyper FDR Qvalue) was used.

(B) Distribution of PSC super enhancers (SEs), as defined by (Whyte et al., 2013), compared with all eTREs in the reactivation clusters.

(C) Heat map indicates the enrichment ( $-\log_{10}(\text{pvalue})$ ) of select TFs at the accessible sites around the TSS ( $\pm 2.5\text{kb}$ ) of gene reactivation clusters as indicated by LOLA analysis (Sheffield and Bock, 2016). Not significant ( $q > 0.001$ ) terms are shown in gray.

(D) Schematic for assigning eTREs to genes based on linear distance (closest eTRE  $\pm 20\text{kb}$  from TSS). Relative enrichment of transcriptional reactivation patterns of paired eTREs and genes using this method. Size of dots indicates p-value (two-sided Fisher's exact test) and color indicates ratio of observed (Obs) versus expected (Exp) frequency.

(E) Schematic for assigning eTREs to genes based on asynchronous PSC H3K27ac HiChIP data (Di Giammartino et al., 2019) at 10kb resolution. Relative enrichment of transcriptional reactivation patterns of paired eTREs and genes using this method. Size of dots indicates p-value (two-sided Fisher's exact test) and color indicates ratio of observed (Obs) versus expected (Exp) frequency.

(F) Median transcriptional reactivation of eTREs overlapping (at least 1bp overlap) with "Retained" and "Lost" H3K27ac, KLF4, and ATAC-seq peaks. eTREs overlapping with both Retained and Lost peaks were assigned to Retained. H3K27AC Retained (n=3826), H3K27AC Lost (n=3463). KLF4 Retained (n=1023), KLF4 Lost (n=2226). ATAC-seq Retained (n=2112), ATAC-seq Lost (n=9155). Error bars show upper and lower limit of 95% confidence interval. Asterisks indicate significance (\*\*\*)  $p < 0.0001$  for Retained vs. Lost, two-sided Wilcoxon's rank sum test.)

See [Table S6](#) for complete statistical analysis for all panels.

Figure S4

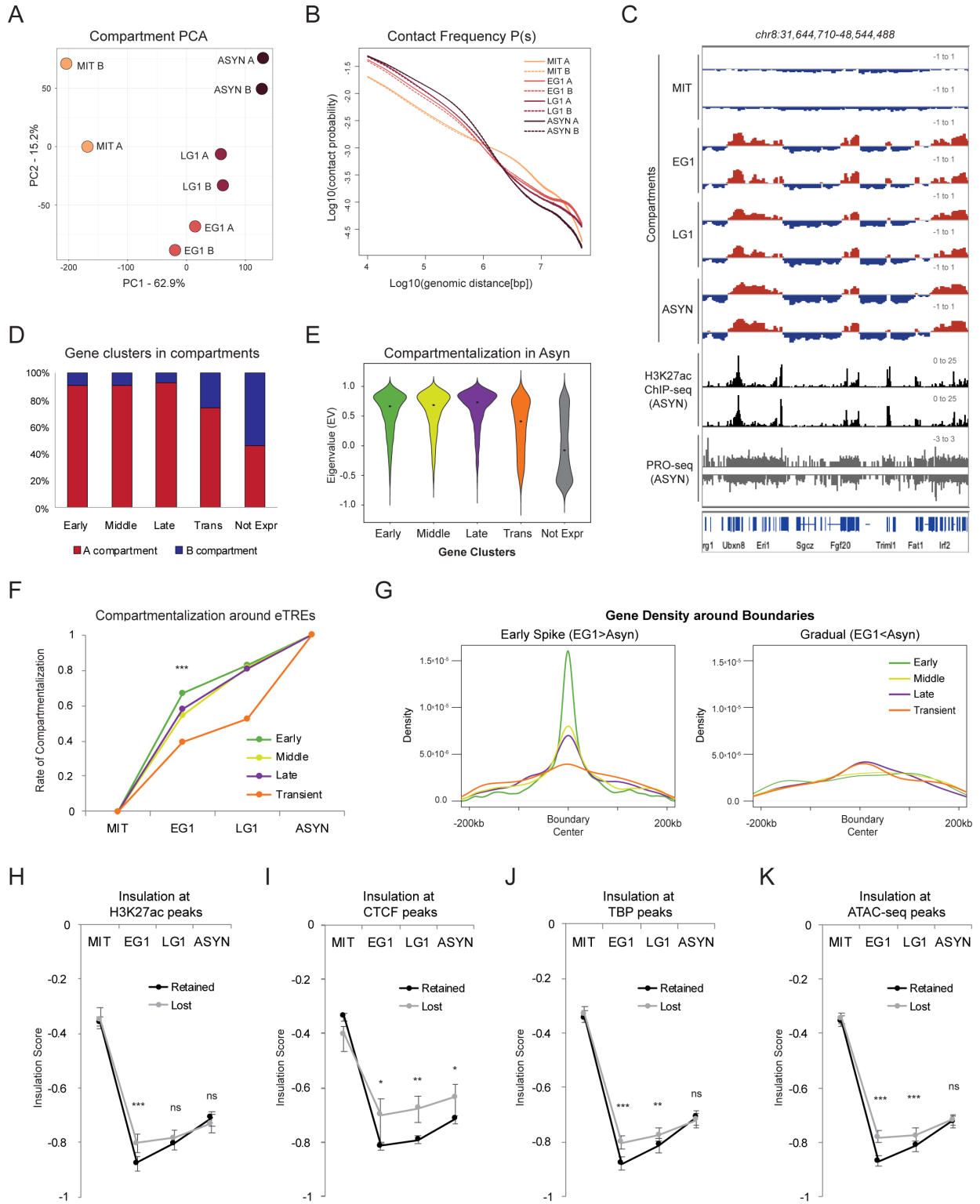


**Figure S4. Hi-C sample QC and correlation of large-scale chromatin with transcriptional resetting and mitotic bookmarking factors (related to Figure 4)**

(A) PCA of Hi-C samples based on compartment eigenvalues (EV) for each 100kb bin.

(B) Contact frequency ( $P$ ) versus genomic distance ( $s$ ) for Hi-C datasets normalized for sequencing depth, shown on a log<sub>10</sub> scale for both axes.

(C) Genome browser tracks of a 17Mb region (*chr8:31,644,710-48,544,488*) showing the compartmentalization (EV) at each time point for both replicates, as well as asynchronous H3K27ac ChIP-seq (Liu et al., 2017b) and asynchronous PRO-seq tracks.

(D) Bar plot showing the percent of the genes in each transcriptional reactivation cluster, as well as the 10564 not expressed (Not Expr) genes, that fall into A and B compartments. A compartments are defined as eigenvalue (EV)>0 in asynchronous cells, while B compartments are EV<0 in asynchronous cells.

(E) Violin plot showing the asynchronous compartment score (eigenvalue, EV) for 100kb bins containing genes in each of the reactivation clusters (Early, Middle, Late, Transient) as well as for not expressed (Not Expr) genes.

(F) Line plot showing rate of compartmentalization during mitotic exit for bins containing eTREs from the four reactivation kinetic clusters (Early, Middle, Late, Transient). Asterisks indicate significance (\*\*\*)  $p < 0.0001$  for Early vs. any other cluster, two-sided Wilcoxon's rank sum test).

(G) Density of the genes from each transcriptional reactivation cluster around TAD boundaries that were rapidly or gradually reset during mitotic exit. All boundaries called at any time point were pooled, and then further filtered to those that were dramatically (difference>0.2) better insulated in EG1 than ASYN ("Early Spike", n=1772) or better insulated in ASYN than EG1 ("Gradual", n=355). Density of the gene clusters is shown +/-200kb around the respective boundary centers.

(H-K) Median insulation score at each time point of TAD boundaries overlapping Retained or Lost bookmarking features. Only TAD boundaries called in asynchronous cells were used, and boundaries containing multiple peak types were prioritized by Retained>Lost. Error bars show upper and lower limit of 95% confidence interval. Asterisks indicate significance (\*  $p < 0.01$ , \*  $p < 0.001$ , \*  $p < 0.0001$  for Retained vs. Lost, two-sided Wilcoxon's



rank sum test). Not significant (ns) indicates  $p > 0.01$ . (H) H3K27ac (I) CTCF (J) TBP and (K) ATAC-seq.

See [Table S6](#) for complete statistical analysis for all panels.

Figure S5

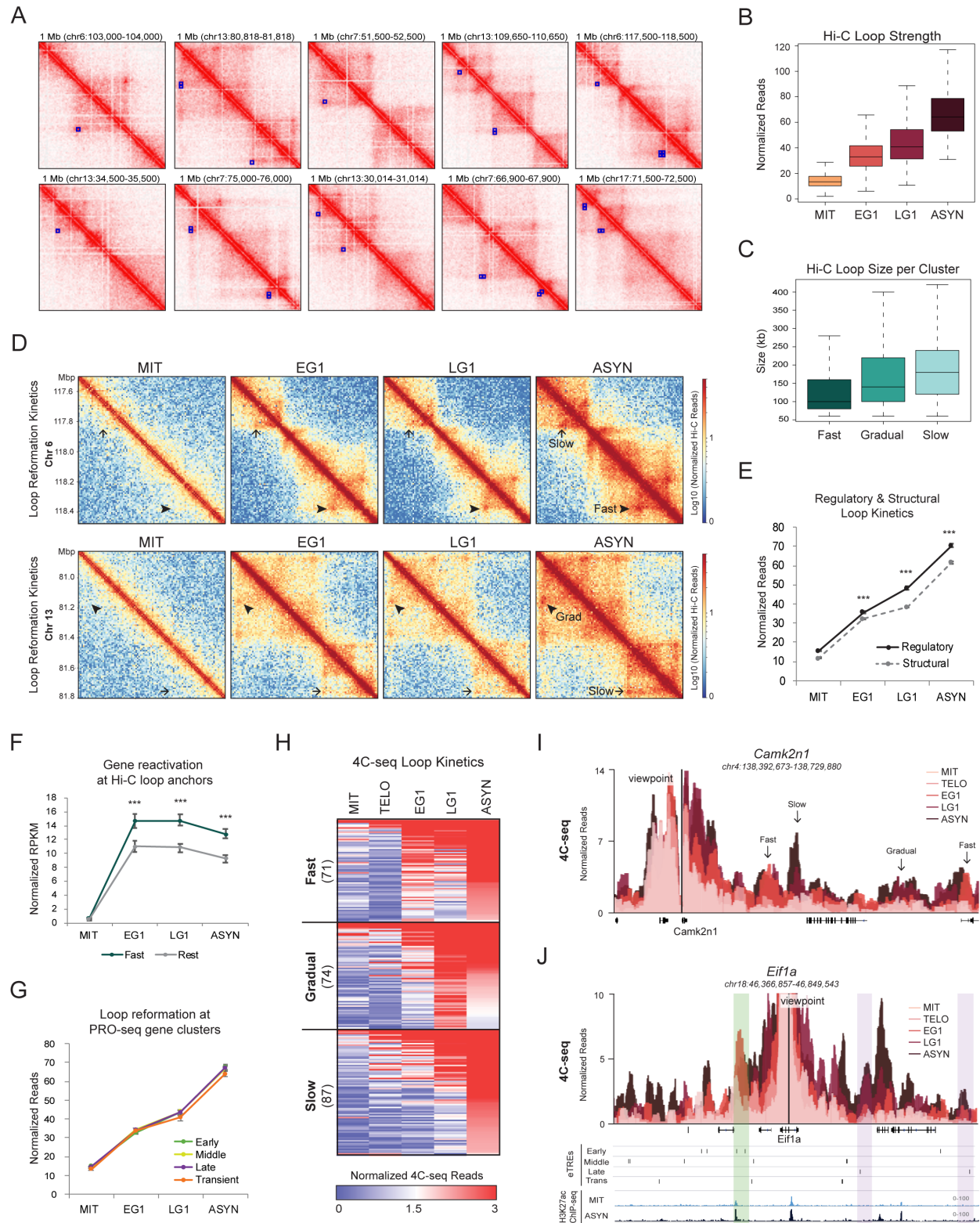


**Figure S5. Examples of high-confidence, filtered Hi-C loops and high-resolution 4C-seq contacts and their reformation kinetics during mitotic exit (related to Figure 5)**

(A) Hi-C interaction maps of ten 1Mb genomics regions at 10kb resolution, visualized using Juicebox (Robinson et al., 2018). For each example, raw Hi-C data from ASYN cells are shown and the 14K refined FitHiC contacts are projected on the left side.

(B) Box plot depicting the contact strength (normalized Hi-C reads) over the time course for all 14,091 high-confidence loops.

(C) Box plot showing median size (distance between anchors) of each Hi-C loop cluster.

(D) Hi-C interaction maps (log<sub>10</sub> Normalized Hi-C reads) of a region on chromosome 6 (*chr6:117,500,000-118,500,000*) and a region on chromosome 13 (*chr13:80,810,000-81,810,000*) at each time point. All images are at 10kb resolution. Examples of Fast, Gradual, and Slow reestablished contacts are indicated.

(E) Reformation kinetics of Regulatory loops (defined by an H3K27ac peak in both anchors) compared with Structural loops (no H3K27ac peaks, but with CTCF and/or Cohesin in at least one anchor). n = 2588 Regulatory, n = 5977 Structural. Error bars show upper and lower limit of 95% confidence interval. Asterisks indicate significance (\*\*\*) p<0.0001 for Regulatory vs. Structural, two-sided Wilcoxon's rank sum test).

(F) Median transcriptional reactivation kinetics for genes within Fast Hi-C loops compared to the Rest (Gradual & Slow Hi-C loops). Anchors in multiple clusters were prioritized Fast>Rest. # of genes: Fast=2482, Rest=3150. Error bars show upper and lower limit of 95% confidence interval. Asterisks indicate significance (\*\*\*) p<0.0001 for Fast vs. Rest, two-sided Wilcoxon's rank sum test).

(G) Loop reformation kinetics around PRO-seq gene reactivation clusters (see Figure 2C). Loops overlapping with multiple gene clusters were prioritized as Early (n=2691 loops) > Middle (n=1922) > Late (n=1255) > Transient (n=685). Error bars show upper and lower limit of 95% confidence interval.

(H) Heat map of the three K-means groups (Fast, Gradual, Slow) for all 232 loops detected by 4C-seq around 11 loci. Heat map shows average 4C-seq counts per million (CPM) over the time course for each contact. Number of loops per group is shown.

(I) 4C-seq data is represented as average CPM around the viewpoint (*Camk2n1* promoter), with each time point shown as an overlapping bar plot. Arrows indicate relevant contacts.

(J) 4C-seq data is represented as average CPM around the viewpoint (*Eif1a* promoter), with each time point shown as an overlapping bar plot. Genome browser tracks underneath show the eTRE reactivation clusters (Early, Middle, Late, and Transient) and H3K27ac ChIP-seq in mitotic and asynchronous cells (Liu et al., 2017b). A fast-reformed region with Early eTREs is highlighted in green while slower reset regions around Late eTREs are highlighted in purple.

See [Table S6](#) for complete statistical analysis for all panels.

Figure S6

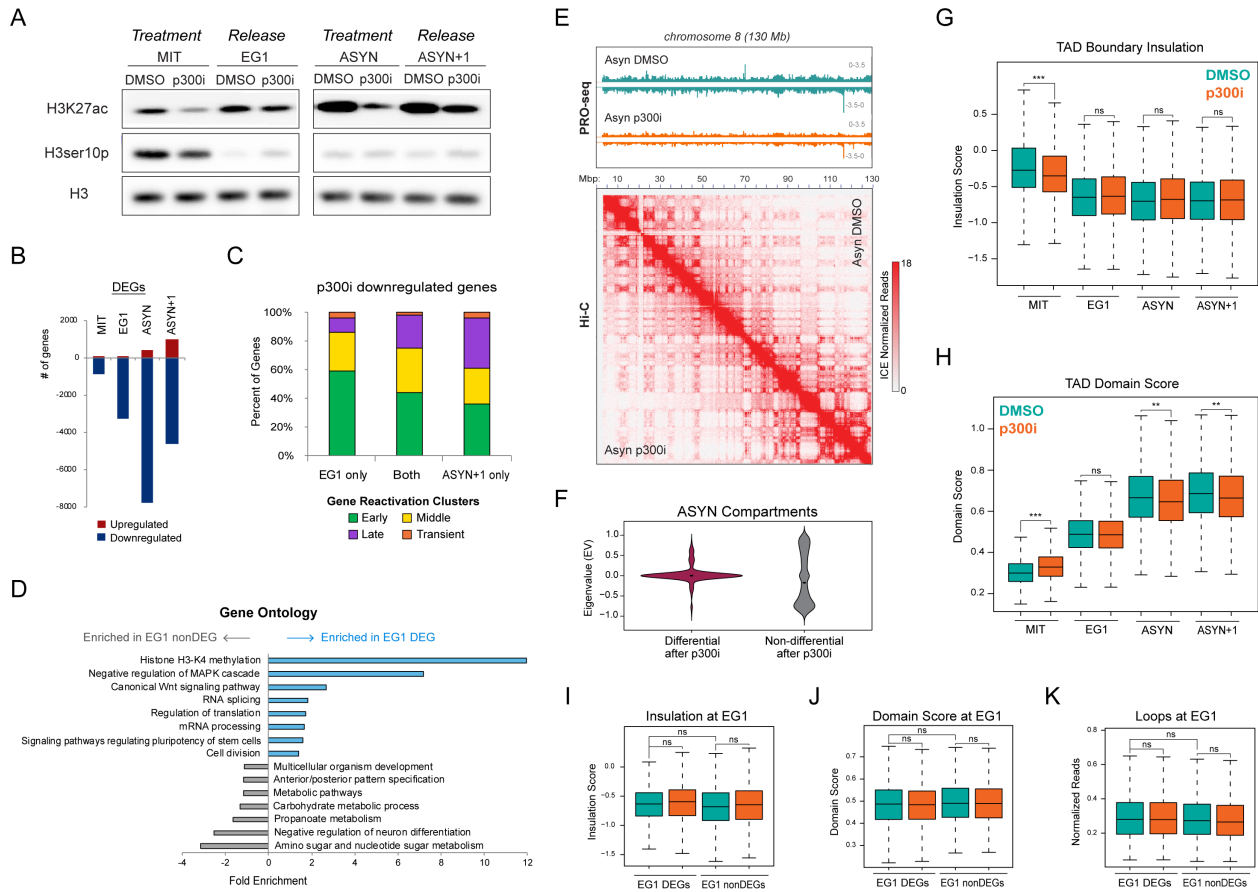


**Figure S6. Further characterization of p300 inhibitor treatment on transcription and 3D chromatin architecture (related to Figure 6)**

(A) Western blot analysis captures the reduction of H3K27ac upon p300i treatment compared to DMSO treated controls and the quick recovery upon release. H3ser10p was used as a marker of mitotic chromatin, while H3 was used as a loading control.

(B) Bar plot indicates the number of upregulated (red) and downregulated (blue) genes when comparing p300i- and DMSO-treated samples at each time point. Differentially expressed genes (DEGs) were called using fold change >1.2 and adjusted p-value <0.05.

(C) Bar plot showing the distribution of the Gene Reactivation clusters (see Figure 2C) within genes histone downregulated after p300i at EG1 only, ASYN+1 only, or Both time points.

(D) Bar plot shows the fold enrichment (EG1 DEG/nonDEG) of selected Gene Ontology (GO) terms. All selected GO terms were significantly enriched (adjusted (Benjamini)

pvalue <0.05) in the gene group (EG1 DEG or nonDEG) that showed a higher fold enrichment.

(E) Genome browser tracks for chromosome 8 (130 Mb) showing the PRO-seq data (merge of triplicates) for ASYN DMSO and ASYN p300i samples, indicating the global decrease in transcription after p300i. Below is the Hi-C contact map for the same region showing no effect on compartmentalization (ASYN DMSO on upper right; ASYN p300i on lower left). Hi-C data was visualized using Juicebox ([Robinson et al., 2018](#)) at 200kb resolution.

(F) Violin plots showing that the few compartments (126 up, 208 down) that were significantly affected ( $\text{diff} > 0.2$ ,  $p < 0.01$ ) by p300i treatment in ASYN cells, have much weaker compartmentalization (Eigenvalue around 0) in steady state (ASYN without treatment) compared to the rest (>98%,  $n = 24,879$ ) that were non-differential between DMSO and p300i.

(G-H) Box plots show TAD boundary insulation (G) and domain score (H) at each time point (MIT, EG1, ASYN, ASYN+1) after DMSO or p300i treatment/recovery. TADs ( $n = 1494$ ) and boundaries ( $n = 2954$ ) common between DMSO and p300i ASYN samples were used for these analyses. Asterisks indicate significance (\*  $p < 0.01$ , \*\*  $p < 0.001$ , \*\*\*  $p < 0.001$ ) for DMSO vs. p300i, two-sided Wilcoxon's rank sum test. Not significant (ns) indicates  $p > 0.01$ .

(I-K) Box plots show TAD boundary insulation (I), TAD domain score (J), and Loop strength (K) during EG1 after DMSO (teal) or p300i (orange) treatment/recovery, focusing specifically around EG1 DEGs and EG1 nonDEGs. Regions containing both EG1 DEGs and nonDEGs were prioritized as DEGs > nonDEGs. Asterisks indicate significance (\*  $p < 0.01$ , \*\*  $p < 0.001$ , \*\*\*  $p < 0.001$ ) for all relevant pairwise comparisons, two-sided Wilcoxon's rank sum test. Not significant (ns) indicates  $p > 0.01$ .

See [Table S6](#) for complete statistical analysis for all panels.

# Figure S7

For Figure S6A

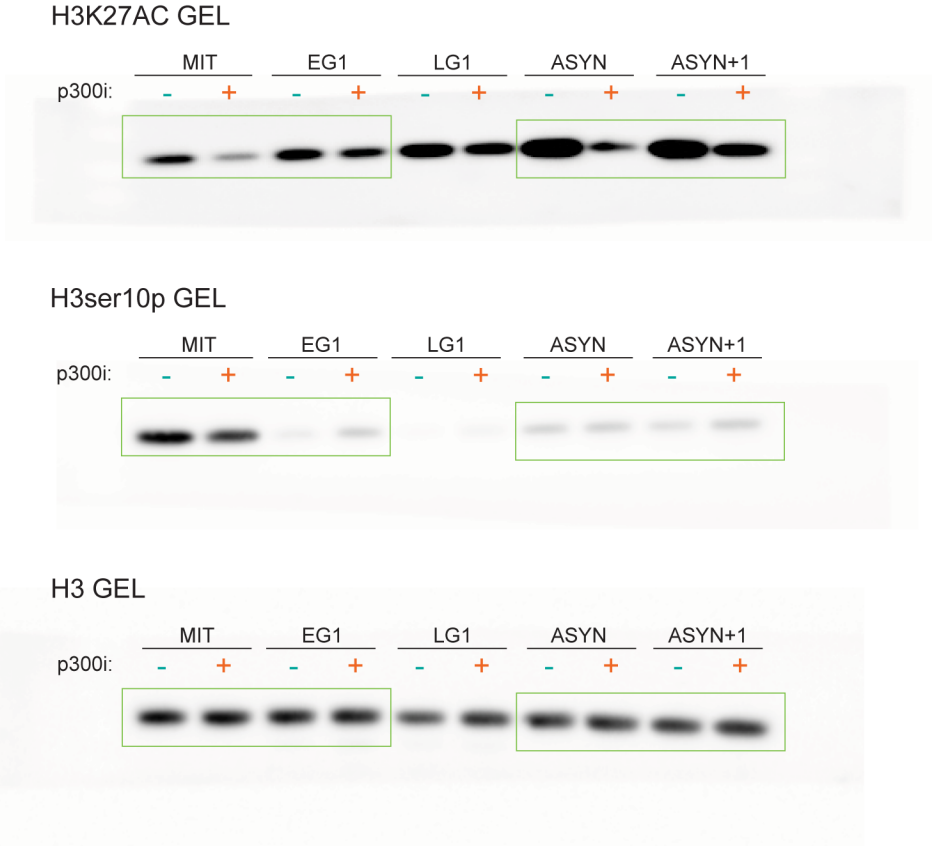


**Figure S7. Raw data for all Western Blot images (related to Figures 6 and S6)**  
Raw Western Blot images, indicating where they were cropped for Figure S6A.